



An enhanced AMLS method and its performance

Jin-Gyun Kim^a, Seung-Hwan Boo^b, Phill-Seung Lee^{b,*}

^a Korea Institute of Machinery and Materials, 156, Gajeongbuk-ro, Yuseong-gu, Daejeon 305-343, Republic of Korea

^b Division of Ocean Systems Engineering, Korea Advanced Institute of Science and Technology, 291 Daehak-ro, Yuseong-gu, Daejeon, 305-701, Republic of Korea

Received 4 July 2014; received in revised form 2 December 2014; accepted 6 January 2015

Available online 13 January 2015

Abstract

In this paper, we present an effective new component mode synthesis (CMS) method based on the concept of the automated multi-level substructuring (AMLS) method. Herein, the original transformation matrix of the AMLS method is enhanced by considering the residual mode effect, and the resulting unknown eigenvalue in the formulation is approximated by employing the idea of the improved reduced system (IRS) method. Using the newly defined transformation matrix, we develop an enhanced AMLS method by which original finite element (FE) models can be more precisely approximated by reduced models, and their solution accuracy is significantly improved. The formulation details of the enhanced AMLS method is presented, and its accuracy and computational cost is investigated through numerical examples.

© 2015 Elsevier B.V. All rights reserved.

Keywords: Structural dynamics; Finite element method; Model reduction; Component mode synthesis; Dynamic substructuring; AMLS method

1. Introduction

While computation capability has increased rapidly, the demand for large scale finite element (FE) models has increased even more rapidly. Therefore, it has always been an important issue to reduce computational cost. A variety of model reduction methods have been developed and widely used in many engineering fields [1–12]. The focus in model reduction is on reducing computational cost with the least possible loss in accuracy.

Within the structural dynamics community, component mode synthesis (CMS) is a popular and effective finite element (FE) model reduction method [5–12]. In CMS methods, an original (global) FE model is partitioned into smaller substructures, substructural eigenvalue problems are solved, and a reduced model constructed by retaining only dominant substructural modes is used for calculations, instead of the much larger original FE model. For this reason, CMS methods can significantly reduce overall computational cost required for many applications (e.g., controller design for multi-body dynamics systems, structural health monitoring, structural design optimization, model identification).

* Corresponding author.

E-mail address: phillseung@kaist.edu (P.-S. Lee).

In the 1990s, the automated multi-level substructuring (AMLS) method, a computer-aided CMS method, was proposed in the field of applied mathematics [13–16]. Due to its computational efficiency, involving recursive partitioning and matrix reordering processes, the AMLS method has become popular for reduced-order modeling. Recently, Beninghof and Lehoucq [17] proposed a well-defined formulation of the AMLS method based on the concept of the Craig–Bampton (CB) method [6,17]. The AMLS method has been also used as a solver of eigenvalue problems in many commercial FE software.

In the original CB and AMLS methods, a transformation matrix is constructed by retaining only dominant substructural modes. Using the transformation matrix, original FE models can be transformed into reduced models, which approximate the original models. With this procedure, residual substructural modes are simply truncated without further consideration. However, when the residual mode effect is considered, the accuracy of the original transformation matrix can be improved. That is, the original (global) models can be more precisely approximated. This approach has been used for flexibility based CMS methods, in which, unlike for the CB and AMLS methods, substructures are connected with a free interface [7,10–12].

In this study, we derive a new transformation matrix for the AMLS method enhanced by considering the residual mode effect. One difficulty is the fact that the enhanced transformation matrix contains an unknown eigenvalue. In order to approximate the unknown eigenvalue, we adopt O’Callahan’s idea, which was originally proposed to develop the improved reduced system (IRS) method by improving Guyan reduction [18]. Finally, the enhanced transformation matrix is defined without the unknown eigenvalue, and by using the newly defined transformation matrix, an enhanced AMLS method is proposed. The reduced FE models obtained from the enhanced AMLS methods have the same size as those obtained from the original AMLS method. However, compared to the original AMLS method, the enhanced AMLS method can provide significantly improved reduced-order models.

In the following sections, we present the general framework of CMS methods in Section 2, and briefly review the original AMLS method in Section 3. In Section 4, the formulation details of the enhanced AMLS method are presented, and its performance and computational cost are tested in Sections 5 and 6, respectively. The conclusions are given in Section 7.

2. Component mode synthesis

In this section, the general framework of component mode synthesis (CMS) is briefly presented. In structural dynamics, the linear dynamics equations of a global (non-partitioned) FE model can be expressed as

$$\mathbf{M}_g \ddot{\mathbf{u}}_g + \mathbf{K}_g \mathbf{u}_g = \mathbf{f}_g, \tag{1}$$

where \mathbf{M}_g and \mathbf{K}_g are the global mass and stiffness matrices, respectively, and \mathbf{u}_g and \mathbf{f}_g are the global displacement and force vectors, respectively. Subscript g denotes the global structure.

Considering a free harmonic vibration ($\mathbf{f}_g = \mathbf{0}$), from Eq. (1), the following eigenvalue problem of the global model is obtained

$$\mathbf{K}_g(\boldsymbol{\varphi}_g)_i = \lambda_i \mathbf{M}_g(\boldsymbol{\varphi}_g)_i, \quad i = 1, 2, \dots, N_g, \quad \text{with } \mathbf{u}_g = \boldsymbol{\Phi}_g \mathbf{q}_g, \tag{2}$$

in which λ_i and $(\boldsymbol{\varphi}_g)_i$ are the global eigenvalue and eigenvector, respectively, and $\boldsymbol{\Phi}_g$ and \mathbf{q}_g are the global eigenvector matrix and its generalized coordinate vector, respectively. N_g is the number of DOFs in the global structure. Note that λ_i is the square of the i th natural frequency (ω_i).

In CMS methods, the global structure is partitioned into substructures as shown in Fig. 1(a), and the eigenvalue analyses of individual substructures are carried out to obtain the dominant substructural modes. Using the dominant substructural modes, the global mass and stiffness matrices in Eq. (2) can be approximated using reduced mass and stiffness matrices.

The eigenvalue problem of the reduced model (reduced eigenvalue problem) is defined as

$$\bar{\mathbf{K}}_p(\bar{\boldsymbol{\varphi}}_p)_i = \bar{\lambda}_i \bar{\mathbf{M}}_p(\bar{\boldsymbol{\varphi}}_p)_i, \quad i = 1, 2, \dots, \bar{N}_p, \quad \text{with } \bar{\boldsymbol{\eta}}_p = \bar{\boldsymbol{\Phi}}_p \bar{\mathbf{q}}_p, \tag{3}$$

where $\bar{\mathbf{M}}_p$ and $\bar{\mathbf{K}}_p$ are the reduced mass and stiffness matrices, respectively, and $\bar{\lambda}_i$ and $(\bar{\boldsymbol{\varphi}}_p)_i$ are the approximated eigenvalue and eigenvector, respectively. The approximated eigenvector matrix $\bar{\boldsymbol{\Phi}}_p$ and its generalized coordinate vector $\bar{\mathbf{q}}_p$ are used to define the approximated global displacement vector $\bar{\boldsymbol{\eta}}_p$. The subscript p denotes the partitioned

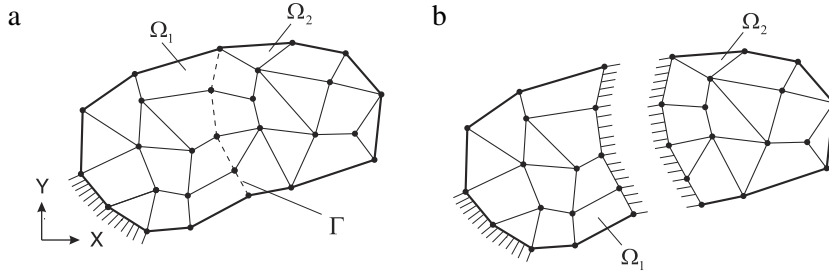


Fig. 1. Partitioned structural model and interface handling in the AMLS method: (a) Partitioned structure, (b) Interface boundary treatment.

structure and an overbar ($\bar{\quad}$) denotes the approximated quantities. The number of DOFs in the reduced model, or the size of the reduced model, is indicated by \bar{N}_p .

Note that, while the formulation details and reduced-order modeling techniques may differ considerably among various CMS methods, the general frameworks are similar.

3. Original AMLS method

Since the AMLS method proposed by Bennighof and his coworkers [17,19,20] is based on the Craig–Bampton (CB) method [6], substructures are connected at a fixed interface boundary, see Fig. 1(b). However, unlike for the CB method, the interface boundary DOFs are also considered as substructures in the AMLS method. The interior DOFs are considered as the bottom level substructures and the interface boundary DOFs are considered as the higher level substructures or highest level substructures. Fig. 2 shows two different partitioned types and the corresponding substructure tree diagrams. The AMLS formulation from previous work [19–21] is used in this paper.

After partitioning a global model into N_s substructures, the mass and stiffness matrices in Eq. (1) are rearranged as

$$\mathbf{M}_g = \begin{bmatrix} \mathbf{M}_1 & & & & \\ & \ddots & & & \\ & & \mathbf{M}_i & \mathbf{M}_{i,j} & \\ & \text{sym.} & & \ddots & \\ & & & & \mathbf{M}_{N_s} \end{bmatrix}, \quad \mathbf{K}_g = \begin{bmatrix} \mathbf{K}_1 & & & & \\ & \ddots & & & \\ & & \mathbf{K}_i & \mathbf{K}_{i,j} & \\ & \text{sym.} & & \ddots & \\ & & & & \mathbf{K}_{N_s} \end{bmatrix},$$

$$\mathbf{u}_g = \begin{bmatrix} \mathbf{u}_1 \\ \vdots \\ \mathbf{u}_i \\ \vdots \\ \mathbf{u}_{N_s} \end{bmatrix}, \quad \mathbf{f}_g = \begin{bmatrix} \mathbf{f}_1 \\ \vdots \\ \mathbf{f}_i \\ \vdots \\ \mathbf{f}_{N_s} \end{bmatrix} \quad \text{for } i, j = 1, 2, \dots, N_s \text{ and } i \neq j, \quad (4)$$

where the diagonal component matrices \mathbf{M}_i and \mathbf{K}_i are the mass and stiffness matrices of the i th substructure, the off-diagonal component matrices $\mathbf{M}_{i,j}$ and $\mathbf{K}_{i,j}$ are the coupling matrices of the i th and j th substructures, and \mathbf{u}_i and \mathbf{f}_i are the displacement and force vectors of the i th substructure, respectively. When the i th and j th substructures are not coupled to each other, $\mathbf{M}_{i,j}$ and $\mathbf{K}_{i,j}$ are zero matrices.

In the AMLS method, the global displacement vector \mathbf{u}_g can be expressed by

$$\mathbf{u}_g = \mathbf{T}_0 \boldsymbol{\eta}_p \quad \text{with } \mathbf{T}_0 = \mathbf{T}^{(1)} \mathbf{T}^{(2)} \dots \mathbf{T}^{(N_s)} = \prod_{i=1}^{N_s} \mathbf{T}^{(i)}, \quad (5)$$

where the transformation matrix \mathbf{T}_0 is given by sequentially multiplying the substructural transformation matrices $\mathbf{T}^{(i)}$ from $\mathbf{T}^{(1)}$ to $\mathbf{T}^{(N_s)}$, and $\boldsymbol{\eta}_p$ is the generalized coordinate vector of the partitioned structure.

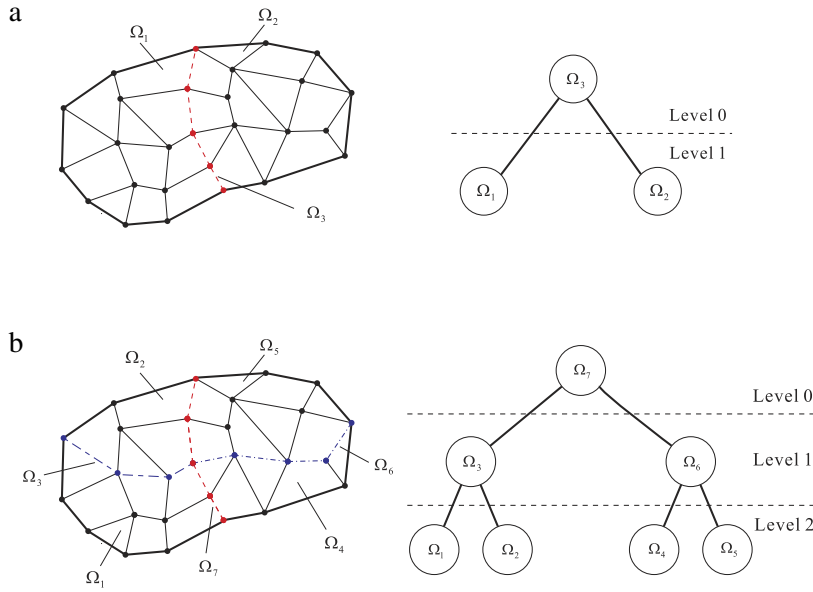


Fig. 2. Substructure tree diagram: (a) Substructural levels 0 and 1, (b) Substructural levels 0, 1 and 2.

Due to the recursive transformation procedures in the AMLS method, the i th incompletely transformed mass and stiffness matrices, $\hat{\mathbf{M}}^{(i)}$ and $\hat{\mathbf{K}}^{(i)}$, are defined by

$$\begin{aligned} \hat{\mathbf{M}}^{(i)} &= \left(\mathbf{T}^{(1)} \mathbf{T}^{(2)} \dots \mathbf{T}^{(i)} \right)^T \mathbf{M}_g \left(\mathbf{T}^{(1)} \mathbf{T}^{(2)} \dots \mathbf{T}^{(i)} \right) \quad \text{and} \\ \hat{\mathbf{K}}^{(i)} &= \left(\mathbf{T}^{(1)} \mathbf{T}^{(2)} \dots \mathbf{T}^{(i)} \right)^T \mathbf{K}_g \left(\mathbf{T}^{(1)} \mathbf{T}^{(2)} \dots \mathbf{T}^{(i)} \right), \quad \text{for } i = 1, 2, \dots, N_s - 1. \end{aligned} \tag{6}$$

In Eq. (6), $\mathbf{T}^{(i)}$ is given by

$$\begin{aligned} \mathbf{T}^{(i)} &= \left[\begin{array}{c|c|c} \mathbf{I} & \mathbf{0} & \mathbf{0} \\ \mathbf{0} & \Phi_i & \Psi_{i,i+1} \cdots \Psi_{i,j} \cdots \Psi_{i,N_s} \\ \mathbf{0} & \mathbf{0} & \mathbf{I} \end{array} \right], \quad \Phi_i = \left[\begin{array}{cc} \Phi_i^d & \Phi_i^r \end{array} \right], \\ \Psi_{i,j} &= -(\hat{\mathbf{K}}_i^{(i-1)})^{-1} (\hat{\mathbf{K}}_{i,j}^{(i-1)}) \quad \text{with } \hat{\mathbf{K}}_{1,j}^{(0)} = \mathbf{K}_{1,j}, \text{ for } i = 1, 2, \dots, N_s \text{ and } j = i + 1, i + 2, \dots, N_s, \end{aligned} \tag{7}$$

in which Φ_i and $\Psi_{i,j}$ are the eigenvector matrix of the i th substructure and the constraint mode matrix to couple the i th and j th substructures, respectively, and $\hat{\mathbf{K}}_i^{(i-1)}$ and $\hat{\mathbf{K}}_{i,j}^{(i-1)}$ are the diagonal and off-diagonal component stiffness matrices of the i th substructure in the $(i - 1)$ th incompletely transformed stiffness matrix $\hat{\mathbf{K}}^{(i-1)}$ defined in Eq. (6). When the i th and j th substructures are not coupled to each other, $\Psi_{i,j}$ is a zero matrix.

It is important to note that the eigenvector matrix Φ_i in Eq. (7) contains the dominant term Φ_i^d and the residual term Φ_i^r . The superscripts d and r denote the dominant and residual terms, respectively.

The eigenvector matrix Φ_i in Eq. (7) is calculated after solving the following substructural eigenvalue problems

$$\hat{\mathbf{K}}_i^{(i-1)} \Phi_i = \Lambda_i \hat{\mathbf{M}}_i^{(i-1)} \Phi_i \quad \text{with } \hat{\mathbf{K}}_1^{(0)} = \mathbf{K}_1, \hat{\mathbf{M}}_1^{(0)} = \mathbf{M}_1 \text{ for } i = 1, 2, \dots, N_s, \tag{8}$$

where Λ_i is the eigenvalue matrix for the i th substructure, and $\hat{\mathbf{M}}_i^{(i-1)}$ is the diagonal component mass matrix of $\hat{\mathbf{M}}^{(i-1)}$ defined in Eq. (6). It should be noted that, to obtain the i th eigenvector matrix Φ_i , the $(i - 1)$ th incompletely transformed mass and stiffness matrices are used.

in which the component matrices are defined by

$$\hat{\Lambda}_d = \Lambda_d - \lambda \mathbf{M}_{dd}, \quad \hat{\Lambda}_r = \Lambda_r - \lambda \mathbf{M}_{rr}, \tag{18a}$$

$$\Lambda_d = (\mathbf{T}_0^d)^T \mathbf{K}_g (\mathbf{T}_0^d), \quad \Lambda_r = (\mathbf{T}_0^r)^T \mathbf{K}_g (\mathbf{T}_0^r), \tag{18b}$$

$$\mathbf{M}_{dd} = (\mathbf{T}_0^d)^T \mathbf{M}_g (\mathbf{T}_0^d), \quad \mathbf{M}_{dr} = (\mathbf{T}_0^d)^T \mathbf{M}_g (\mathbf{T}_0^r), \quad \mathbf{M}_{rr} = (\mathbf{T}_0^r)^T \mathbf{M}_g (\mathbf{T}_0^r). \tag{18c}$$

Then, Eq. (17a) can be rewritten in a component matrix form

$$\begin{bmatrix} \hat{\Lambda}_d & -\lambda \mathbf{M}_{dr} \\ -\lambda \mathbf{M}_{dr}^T & \hat{\Lambda}_r \end{bmatrix} \begin{bmatrix} \boldsymbol{\eta}_p^d \\ \boldsymbol{\eta}_p^r \end{bmatrix} = \mathbf{0}. \tag{19}$$

Using the second row in Eq. (19), the following relation is obtained

$$\boldsymbol{\eta}_p^r = \lambda \hat{\Lambda}_r^{-1} \mathbf{M}_{dr}^T \boldsymbol{\eta}_p^d. \tag{20}$$

Substituting Eq. (20) into Eq. (16), the global displacement vector \mathbf{u}_g can be represented by

$$\mathbf{u}_g = \left[\mathbf{T}_0^d + \lambda \mathbf{T}_0^r \hat{\Lambda}_r^{-1} \mathbf{M}_{dr}^T \right] \boldsymbol{\eta}_p^d. \tag{21}$$

Using $\mathbf{T}_0^r = \hat{\Psi} \Phi_r$ (see Eq. (16)) and $\mathbf{M}_{dr} = (\mathbf{T}_0^d)^T \mathbf{M}_g (\mathbf{T}_0^r)$ (see Eq. (18c)) in Eq. (21), we obtain

$$\mathbf{u}_g = \mathbf{T}_0^d \boldsymbol{\eta}_p^d + \lambda \hat{\Psi} \hat{\mathbf{F}}_r \hat{\Psi}^T \mathbf{M}_g \mathbf{T}_0^d \boldsymbol{\eta}_p^d, \tag{22}$$

with

$$\hat{\mathbf{F}}_r = \Phi_r \hat{\Lambda}_r^{-1} \Phi_r^T = \Phi_r [\Lambda_r - \lambda \mathbf{M}_{rr}]^{-1} \Phi_r^T, \tag{23}$$

where $\hat{\mathbf{F}}_r$ is the residual flexibility of substructures.

Using Taylor expansion, $\hat{\mathbf{F}}_r$ can be written as

$$\begin{aligned} \hat{\mathbf{F}}_r &= \Phi_r [\Lambda_r - \lambda \mathbf{M}_{rr}]^{-1} \Phi_r^T \\ &= \Phi_r \Lambda_r^{-1} \Phi_r^T + \lambda \Lambda_r^{-1} \mathbf{M}_{rr} \Lambda_r^{-1} \Phi_r^T + O(\lambda^2) + O(\lambda^3) + \dots \end{aligned} \tag{24}$$

Using Eq. (24) in Eq. (22), and truncating terms of higher order than λ , we can obtain the approximated global displacement vector $\bar{\mathbf{u}}_g$ as follows:

$$\mathbf{u}_g \approx \bar{\mathbf{u}}_g = \bar{\mathbf{T}}_1 \boldsymbol{\eta}_p^d, \quad \bar{\mathbf{T}}_1 = \bar{\mathbf{T}}_0 + \bar{\mathbf{T}}_r, \tag{25a}$$

$$\bar{\mathbf{T}}_0 = \mathbf{T}_0^d, \quad \bar{\boldsymbol{\eta}}_p = \boldsymbol{\eta}_p^d, \quad \bar{\mathbf{T}}_r = \lambda \hat{\Psi} \mathbf{F}_{rs} \hat{\Psi}^T \mathbf{M}_g \mathbf{T}_0^d, \quad \mathbf{F}_{rs} = \Phi_r \Lambda_r^{-1} \Phi_r^T, \tag{25b}$$

where $\bar{\mathbf{T}}_1$ is the transformation matrix enhanced by $\bar{\mathbf{T}}_r$, and \mathbf{F}_{rs} is the zeroth order term (or static part) of the residual flexibility $\hat{\mathbf{F}}_r$. Here, \mathbf{F}_{rs} is indirectly calculated using full and dominant flexibility without considering the residual substructural modes as

$$\mathbf{F}_{rs} = \Phi_r \Lambda_r^{-1} \Phi_r^T = \begin{bmatrix} \mathbf{F}_1^{rs} & & & & \\ & \ddots & & & \\ & & \mathbf{F}_i^{rs} & & \mathbf{0} \\ & & & \ddots & \\ \mathbf{0} & & & & \mathbf{F}_{N_s-1}^{rs} \\ & & & & & \mathbf{0} \end{bmatrix}, \tag{26}$$

$$\mathbf{F}_i^{rs} = (\hat{\mathbf{K}}_i^{(i-1)})^{-1} - (\Phi_i^d)^T (\Lambda_i^d)^{-1} (\Phi_i^d)^T, \quad \text{for } i = 1, 2, \dots, N_s - 1,$$

Table 1
Comparison between the original and enhanced AMLS methods.

	Original AMLS	Enhanced AMLS
Transformation matrix	$\bar{\mathbf{T}}_0 = \hat{\Psi} \Phi_d$	$\bar{\mathbf{T}}_1 = \bar{\mathbf{T}}_0 + \bar{\mathbf{T}}_r = \bar{\mathbf{T}}_0 + \hat{\Psi} \mathbf{F}_{rs} \hat{\Psi}^T \mathbf{M}_g \bar{\mathbf{T}}_0 \bar{\mathbf{M}}_p^{-1} \bar{\mathbf{K}}_p$
Reduced mass matrix	$\bar{\mathbf{M}}_p$	$\bar{\mathbf{M}}_p + \bar{\mathbf{T}}_r^T \mathbf{M}_g \bar{\mathbf{T}} + \bar{\mathbf{T}}_0^T \mathbf{M}_g \bar{\mathbf{T}}_r + \bar{\mathbf{T}}_r^T \mathbf{M}_g \bar{\mathbf{T}}_r$
Reduced stiffness matrix	$\bar{\mathbf{K}}_p$	$\bar{\mathbf{K}}_p + \bar{\mathbf{T}}_r^T \mathbf{K}_g \bar{\mathbf{T}}_0 + \bar{\mathbf{T}}_0^T \mathbf{K}_g \bar{\mathbf{T}}_r + \bar{\mathbf{T}}_r^T \mathbf{K}_g \bar{\mathbf{T}}_r$
Size of the reduced matrices	\bar{N}_p	\bar{N}_p

in which $(\hat{\mathbf{K}}_i^{(i-1)})^{-1}$ and $(\Phi_i^d)(\Lambda_i^d)^{-1}(\Phi_i^d)^T$ are the full and dominant flexibility matrices for the i th substructure. Note that the enhanced transformation matrix $\bar{\mathbf{T}}_1$ defined in Eq. (25) has been also employed to develop an error estimator of the original AMLS method [21].

Since the eigenvalue λ in $\bar{\mathbf{T}}_r$ is unknown, the enhanced transformation matrix $\bar{\mathbf{T}}_1$ cannot be used to improve the original AMLS method in its present form. To handle this problem, we employ O’Callahan’s approach, which was proposed to improve Guyan reduction [18]. From Eq. (11) with $\mathbf{f}_p = \mathbf{0}$ and $\hat{\mathbf{h}}_p = -\lambda \bar{\mathbf{h}}_p$, the following relation is obtained

$$\lambda \bar{\mathbf{h}}_p = \bar{\mathbf{M}}_p^{-1} \bar{\mathbf{K}}_p \bar{\mathbf{h}}_p, \tag{27}$$

and using Eq. (27) in Eq. (25), $\bar{\mathbf{T}}_r$ is newly defined by

$$\bar{\mathbf{T}}_r = \hat{\Psi} \mathbf{F}_{rs} \hat{\Psi}^T \mathbf{M}_g \bar{\mathbf{T}}_0 \bar{\mathbf{M}}_p^{-1} \bar{\mathbf{K}}_p. \tag{28}$$

Using the redefined $\bar{\mathbf{T}}_r$ in Eq. (28), $\bar{\mathbf{T}}_1$ can be expressed without the unknown eigenvalue λ , and then, new reduced mass and stiffness matrices, denoted by tilde ($\tilde{}$), are defined as

$$\tilde{\mathbf{M}}_p = \bar{\mathbf{T}}_1^T \mathbf{M}_g \bar{\mathbf{T}}_1 = \bar{\mathbf{M}}_p + \bar{\mathbf{T}}_r^T \mathbf{M}_g \bar{\mathbf{T}}_0 + \bar{\mathbf{T}}_0^T \mathbf{M}_g \bar{\mathbf{T}}_r + \bar{\mathbf{T}}_r^T \mathbf{M}_g \bar{\mathbf{T}}_r, \tag{29a}$$

$$\tilde{\mathbf{K}}_p = \bar{\mathbf{T}}_1^T \mathbf{K}_g \bar{\mathbf{T}}_1 = \bar{\mathbf{K}}_p + \bar{\mathbf{T}}_r^T \mathbf{K}_g \bar{\mathbf{T}}_0 + \bar{\mathbf{T}}_0^T \mathbf{K}_g \bar{\mathbf{T}}_r + \bar{\mathbf{T}}_r^T \mathbf{K}_g \bar{\mathbf{T}}_r. \tag{29b}$$

Due to the compensation of the residual mode effects in $\bar{\mathbf{T}}_r$, the reduced mass and stiffness matrices in Eq. (29) are more precisely constructed than the original reduced matrices in Eq. (11). Table 1 shows the comparison of the original and enhanced AMLS methods. Note that it is also possible to consider higher order terms of λ in the enhanced AMLS formulation but there is little additional improvement in solution accuracy.

It is important to note that both methods produce reduced models that have the same size (\bar{N}_p). Unlike in the original AMLS method, \mathbf{F}_{rs} and the inverse of the reduced mass matrix $\bar{\mathbf{M}}_p$ are additionally computed in the enhanced AMLS method. \mathbf{F}_{rs} can be simply calculated by reusing $(\hat{\mathbf{K}}_i^{(i-1)})^{-1}$ in Eq. (7) and the dominant modes. Furthermore, the size of the reduced mass matrix $\bar{\mathbf{M}}_p$ is also much smaller than the original mass matrix \mathbf{M}_g . For these reasons, the additional computational cost of the enhanced AMLS method is not very high.

However, while the transformation matrix $\bar{\mathbf{T}}_0$ of the original AMLS method is sparse, the transformation matrix $\bar{\mathbf{T}}_1$ of the enhanced AMLS method is fully populated. Therefore, the computational cost for the enhanced AMLS method could increase more rapidly than the original AMLS method does, as the size of finite element models becomes larger. However, to achieve a given solution accuracy, the enhanced AMLS method requires smaller reduced models than the original AMLS method, that is, the computational cost can be reduced for reduced models with similar accuracy. In order to clarify this issue, rigorous numerical tests need to be performed considering FE models of various sizes.

In this study, we considered only undamped structural models, but the enhanced AMLS method can be also employed for model reductions of damped structural models [22].

5. Numerical examples

In this section, we compare the performance of the enhanced AMLS method to the original AMLS method. The original and enhanced AMLS methods were implemented using MATLAB. Four structural problems are considered: rectangular plate, cylindrical solid, bench corner structure and hyperboloid shell problems, in which, for finite element modeling, 4-node MITC shell [23–26] and 8-node brick finite elements are used.

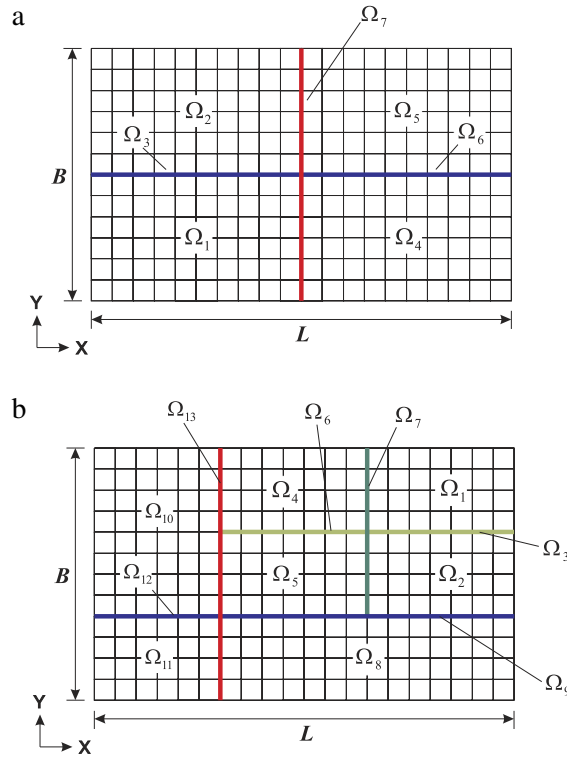


Fig. 3. Rectangular plate problem: (a) Partition Type A, (b) Partition Type B.

The frequency cut-off mode selection method is used to select the dominant modes, and the following relative eigenvalue error is used to measure the accuracy of the original and enhanced AMLS methods.

$$\xi_i = \frac{\bar{\lambda}_i - \lambda_i}{\lambda_i}, \quad (30)$$

in which ξ_i denotes the relative eigenvalue error for the i th mode and the exact global eigenvalue λ_i is obtained from the eigenvalue problem of the global structure in Eq. (2). In the following numerical examples, rigid body modes are not considered for the relative eigenvalue error.

5.1. Rectangular plate problem

We here consider a rectangular plate with free boundary as shown in Fig. 3. Length L is 20.0 m, width B is 12.0 m, and thickness h is 0.08 m. Young's modulus E is 206 GPa, Poisson's ratio ν is 0.33, density ρ is 7850 kg/m³. The plate is modeled by a 20×12 mesh of the 4-node MITC shell finite elements and the number of total DOFs for this problem is 1365. Two different partition types are considered as in Figs. 3(a) and (b):

- Partition Type A: The global structure is partitioned into seven substructures with three substructural levels (levels 0, 1 and 2), see Fig. 3(a). Retaining 30 and 50 dominant modes ($N_d = 30$ and $N_d = 50$), two numerical cases are considered.
- Partition Type B: As shown in Fig. 3(b), the number of substructures is 13 and the number of substructural levels is five (levels 0, 1, 2, 3 and 4). We retain 55 and 75 dominant modes for two numerical cases ($N_d = 55$ and $N_d = 75$).

The numbers of retained substructural modes N_i^d in both partitioned types are listed in Tables 2 and 3 in detail. Figs. 4 and 5 present the relative eigenvalue errors obtained by the original and enhanced AMLS methods. The results show that the enhanced AMLS method significantly outperforms the original AMLS method.

Table 2

Retained mode numbers N_i^d for the rectangular plate problem with Partition Type A. All the substructural modes are retained in the highest level substructure (level 0).

Substructural level	Substructural number	N_i^d	Case 1	Case 2
Level 0	7	N_7^d	65	65
Level 1	3	N_3^d	3	5
	6	N_6^d	3	5
Level 2	1	N_1^d	6	10
	2	N_2^d	6	10
	4	N_4^d	6	10
	5	N_5^d	6	10
Total retained mode number		N_d	30	50
Size of the reduced model		\bar{N}_p	95	115

Table 3

Retained mode numbers N_i^d for the rectangular plate problem with Partition Type B. All the substructural modes are retained in the highest level substructure (level 0).

Substructural level	Substructural number	N_i^d	Case 1	Case 2
Level 0	13	N_{13}^d	65	65
Level 1	9	N_9^d	10	13
	12	N_{12}^d	4	5
Level 2	7	N_7^d	5	7
	8	N_8^d	9	12
	10	N_{10}^d	6	10
	11	N_{11}^d	3	5
Level 3	3	N_3^d	5	5
	6	N_6^d	3	3
Level 4	1	N_1^d	4	6
	2	N_2^d	2	3
	4	N_4^d	3	4
	5	N_5^d	1	2
Total retained mode number		N_d	55	75
Size of the reduced model		\bar{N}_p	120	140

5.2. Cylindrical panel problem

The performance of the proposed method is also tested in a cylindrical panel with free boundary, see Fig. 6. Length L is 0.8 m, radius R is 0.5 m, and thickness h is 0.005 m. Young’s modulus E is 69 GPa, Poisson’s ratio ν is 0.35, and density ρ is 2700 kg/m³. The cylindrical panel is modeled by a 16 × 16 distorted mesh of shell finite elements and each edge is discretized in the following ratio: $L_1 : L_2 : L_3 : \dots : L_{16} = 16 : 15 : 14 : \dots : 1$ [25].

The global structure is partitioned into seven substructures with three substructural levels (levels 0, 1 and 2) as shown in Fig. 6. The numbers of retained substructural modes N_i^d are listed in Table 4. The significant accuracy improvement is observed in the enhanced AMLS method, see Fig. 7.

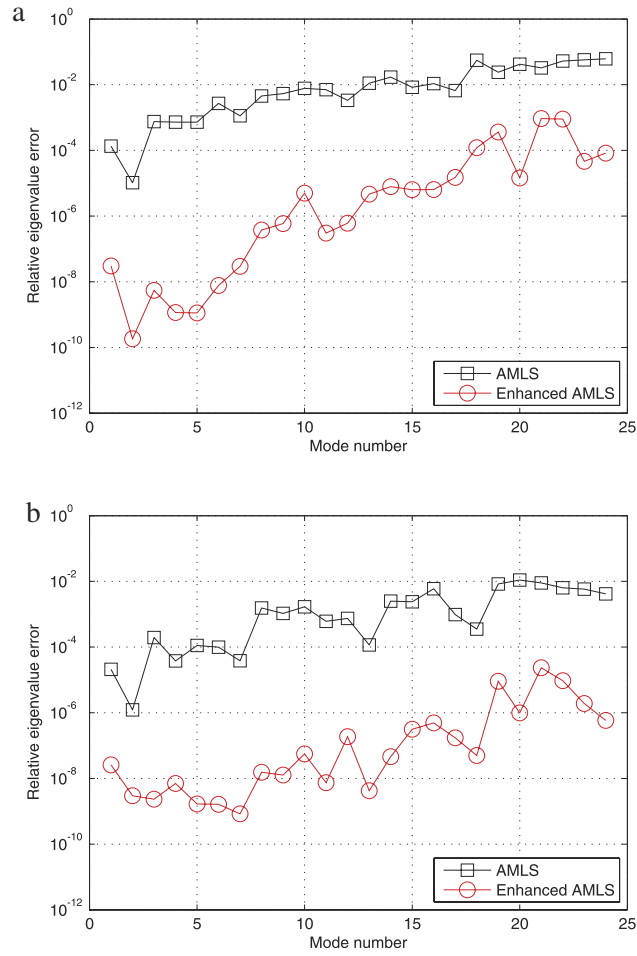


Fig. 4. Relative eigenvalue errors for the rectangular plate problem with the Partition Type A: (a) $N_d = 30$, (b) $N_d = 50$.

Table 4

Retained mode numbers N_i^d for the cylindrical panel problem with a distorted mesh, Partition Type A is applied. All the substructural modes are retained in the highest level substructure (level 0).

Substructural level	Substructural number	N_i^d	Case 1	Case 2
Level 0	7	N_7^d	85	85
Level 1	3	N_3^d	7	11
	6	N_6^d	7	11
Level 2	1	N_1^d	4	10
	2	N_2^d	14	29
	4	N_4^d	14	29
	5	N_5^d	4	10
Total retained mode number		N_d	50	100
Size of the reduced model		\bar{N}_p	135	185

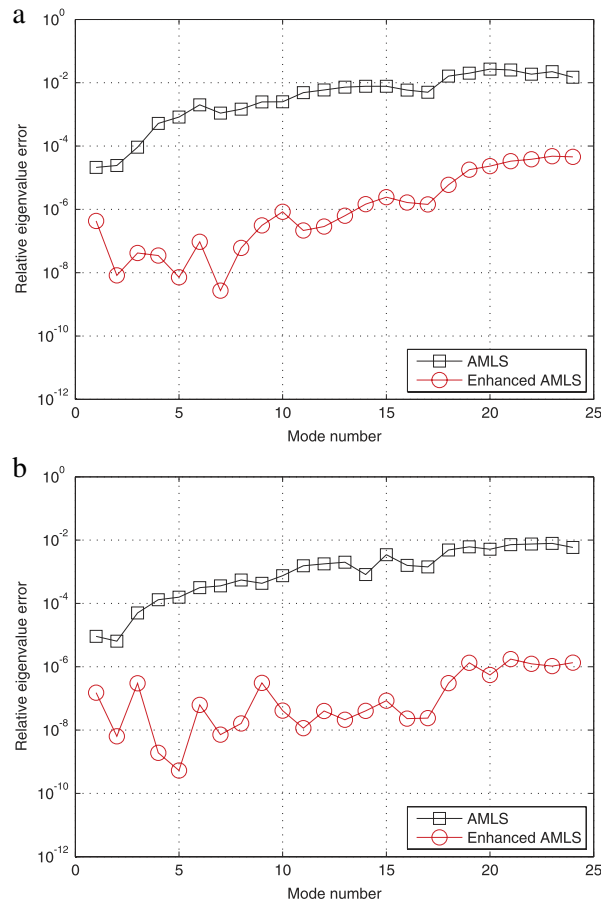


Fig. 5. Relative eigenvalue errors for the rectangular plate problem with Partition Type B: (a) $N_d = 55$, (b) $N_d = 75$.

5.3. Cylindrical solid problem

Let us consider a cylindrical solid problem with free boundary at both ends, see Fig. 8. Lengths L_1 and L_2 are 0.16 and 0.24 m, respectively, and the radii R_1 , R_2 and R_3 are 0.08 m, 0.12 m, and 0.16 m, respectively. Young’s modulus E is 76 GPa, Poisson’s ratio ν is 0.33, and density ρ is 2796 kg/m^3 . The cylindrical solid problem is modeled using 8-node brick elements and the number of total DOFs is 1740. Considering the three substructural levels (0, 1 and 2), the global structure is partitioned into seven substructures. Two different numbers of retained dominant modes ($N_d = 70$ and $N_d = 120$) are considered as listed in Table 5. The relative eigenvalue errors are plotted in Fig. 9. The results show the robustness of the enhanced AMLS method compared with the original AMLS method.

5.4. Bench corner structure problem

Here, a bench corner structure is considered. Lengths L_1 and L_2 are 4.0 m and 1.0 m, heights H_1 and H_2 are 2.0 m and 1.0 m. Width B is 1.0 m and thickness h is 0.025 m. Young’s modulus E is 210 GPa, Poisson’s ratio ν is 0.30, and density ρ is 7850 kg/m^3 . The 4-node MITC shell finite elements are used for the finite element model of the structure, in which the number of DOFs is 3508 DOFs. As shown in Fig. 10, the global structure is partitioned into nine substructures with four sub-structural levels (0, 1, 2 and 3). We retain 50 and 80 dominant modes in two numerical cases ($N_d = 50$ and $N_d = 80$), and the numbers of the retained substructural modes N_i^d are listed in Table 6. Fig. 11 demonstrates the excellent performance of the enhanced AMLS method.

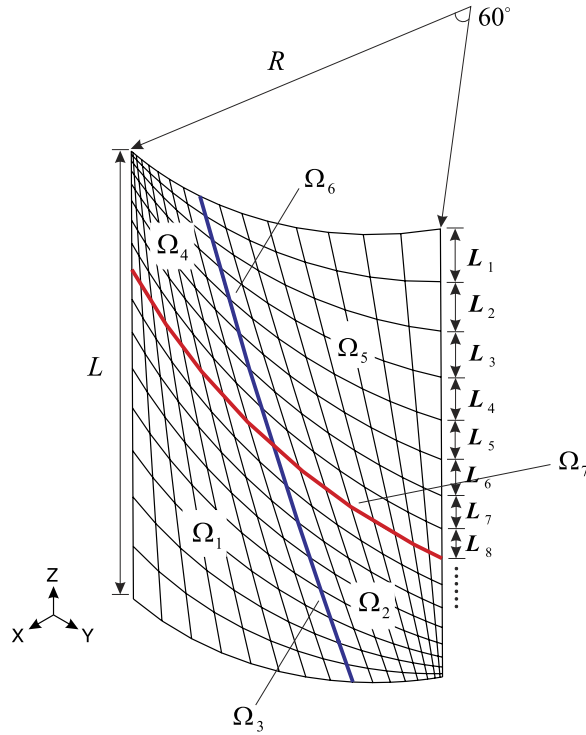


Fig. 6. Cylindrical panel problem with a distorted mesh.

Table 5

Retained mode numbers N_i^d for the cylindrical solid problem. All the substructural modes are retained in the highest level substructure (level 0).

Substructural level	Substructural number	N_i^d	Case 1	Case 2
Level 0	7	N_7^d	180	180
Level 1	3	N_3^d	12	20
	6	N_6^d	10	12
Level 2	1	N_1^d	13	26
	2	N_2^d	13	26
	4	N_4^d	11	18
	5	N_5^d	11	18
Total retained mode number		N_d	70	120
Size of the reduced model		\tilde{N}_p	250	300

5.5. Hyperboloid shell problem

Consider a hyperboloid shell problem of height $H = 4.0$ m and thickness $h = 0.05$ m. The mid-surface of this shell structure is described [25] as

$$x^2 + y^2 = 2 + z^2; \quad z \in [-2, 2]. \tag{31}$$

No boundary condition is imposed. Young’s modulus E is 69 GPa, Poisson’s ratio ν is 0.35, and density ρ is 2700 kg/m³. A 20 (axial) \times 40 (circumferential) mesh of shell finite elements is used. Considering three sub-structural levels (0, 1 and 2), the global structure is partitioned into seven substructures, see Fig. 12. We use 60 and 120 retained

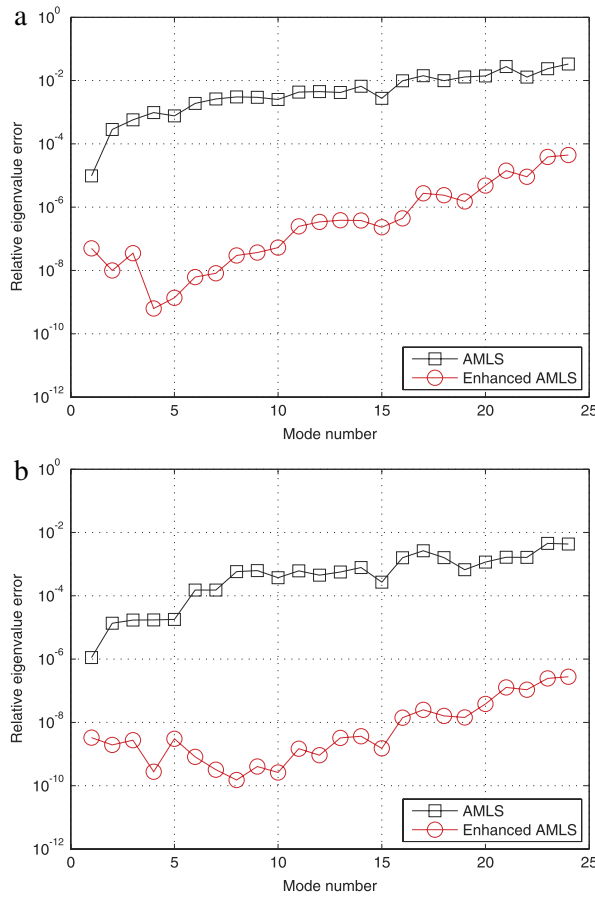


Fig. 7. Relative eigenvalue errors for the cylindrical panel problem with a distorted mesh: (a) $N_d = 50$, (b) $N_d = 100$.

Table 6

Retained mode numbers N_i^d for the bench corner structure problem. All the substructural modes are retained in the highest level substructure (level 0).

Substructural level	Substructural number	N_i^d	Case 1	Case 2
Level 0	9	N_9^d	97	97
Level 1	5	N_5^d	7	11
	8	N_8^d	8	10
	3	N_3^d	5	6
Level 2	4	N_4^d	11	14
	6	N_6^d	2	7
	7	N_7^d	11	18
Level 3	1	N_1^d	4	9
	2	N_2^d	2	5
Total retained mode number		N_d	50	80
Size of the reduced model		\bar{N}_p	147	177

dominant modes in two numerical cases ($N_d = 60$, $N_d = 120$), and the numbers of the retained sub-structural modes N_i^d are listed in Table 7. Fig. 13 consistently demonstrates the excellent performance of the enhanced AMLS method.

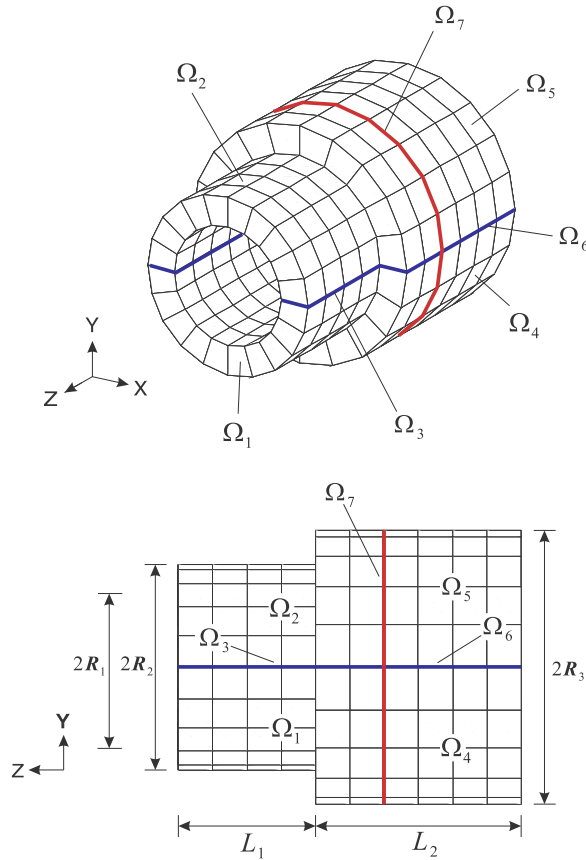


Fig. 8. Cylindrical solid problem.

Table 7

Retained mode numbers N_i^d for the hyperboloid shell problem. All the substructural modes are retained in the highest level substructure (level 0).

Substructural level	Substructural number	N_i^d	Case 1	Case 2
Level 0	7	N_7^d	200	200
Level 1	3	N_3^d	8	14
	6	N_6^d	8	14
Level 2	1	N_1^d	11	23
	2	N_2^d	11	23
	4	N_4^d	11	23
	5	N_5^d	11	23
	Total retained mode number		N_d	60
Size of the reduced model		\bar{N}_p	260	320

6. Computational cost

In order to investigate the computational cost required for the enhanced AMLS method, computation times are measured, and compared with those of the original AMLS method. A sparse matrix computation with MATLAB is

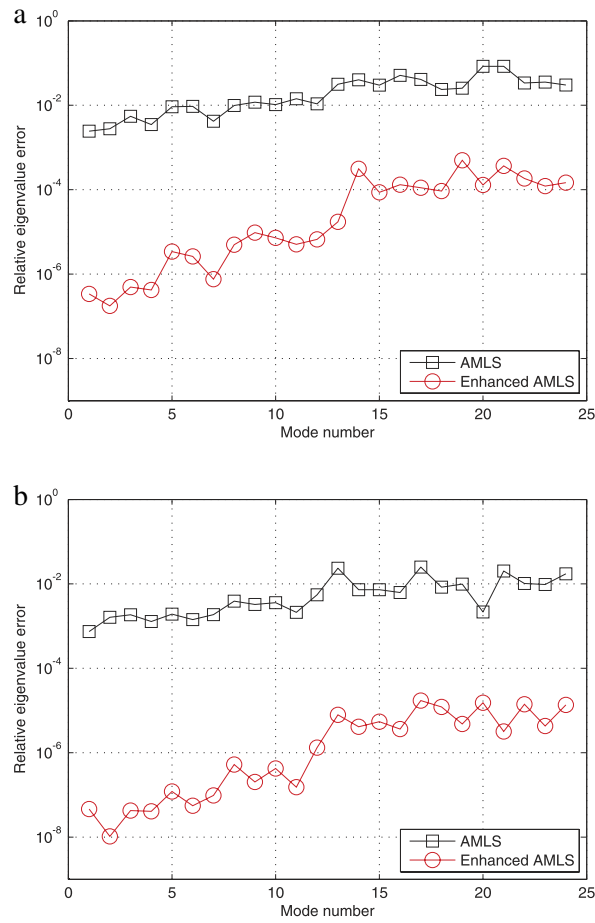


Fig. 9. Relative eigenvalue errors for the cylindrical solid problem: (a) $N_d = 70$, (b) $N_d = 120$.

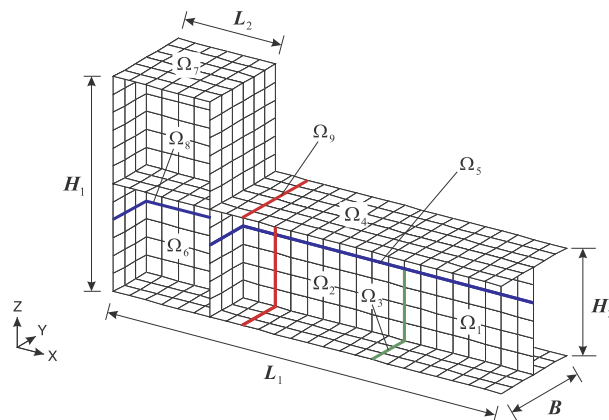


Fig. 10. Bench corner structure problem.

used in a personal computer (Intel core (TM) i7-3770, 3.40 GHz CPU, 16GB RAM). Note that, of course, computation times vary depending on implementation details of the computer codes, as well as on the performance of the computers used. Therefore, the results discussed in this section could not be simply generalized.

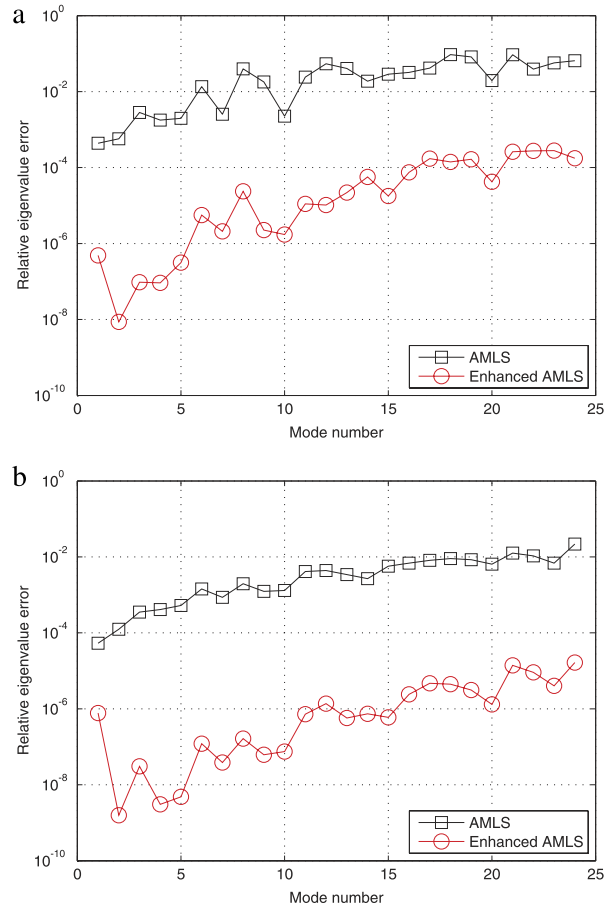


Fig. 11. Relative eigenvalue errors for the bench corner structure problem: (a) $N_d = 50$, (b) $N_d = 80$.

Table 8

Computation times for calculating the lowest eigenvalues by the original and enhanced AMLS methods.

	DOFs		Computation time (s)	
	N_g	N_p	Original AMLS	Enhanced AMLS
Rectangular plate (Freq. cut-off, $N_d = 30$)	1365	135	1.018E-01	1.182E-01
Cylindrical solid (Freq. cut-off, $N_d = 70$)	1740	250	2.912E-01	3.001E-01
Bench corner structure (Freq. cut-off, $N_d = 50$)	3508	147	2.216E-01	2.458E-01
Hyperboloid shell (Freq. cut-off, $N_d = 60$)	4200	260	5.045E-01	5.248E-01

6.1. Reduced models with same size

When the size of the reduced model is the same, additional computation is required for the enhanced AMLS method, compared with the original AMLS method. Table 8 presents the computation times for calculating the lowest eigenvalues (mode number = 1) in the four numerical examples considered in Section 5. Note that the original and enhanced reduced transformation matrices in Eqs. (11) and (29) are used in the original and enhanced AMLS methods, respectively. The results show that the additional computational cost for the enhanced AMLS method is not high compared with the original AMLS method.

We investigate the additional computation times required for the enhanced AMLS method by increasing the number of DOFs in the rectangular plate problem with Partition Type A in Fig. 3(a). We here consider six different meshes: 20×12 ($N_g = 1365$, $N_p = 95$), 30×18 ($N_g = 2945$, $N_p = 125$), 40×24 ($N_g = 5125$, $N_p = 155$), 48×30

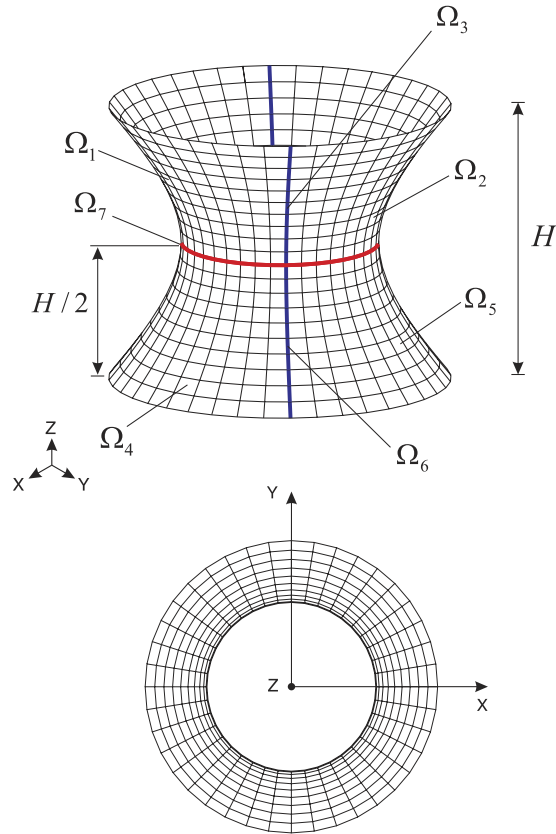


Fig. 12. Hyperboloid shell problem.

($N_g = 7595, \bar{N}_p = 185$), 54×32 ($N_g = 9075, \bar{N}_p = 195$), and 60×36 ($N_g = 11285, \bar{N}_p = 215$), see Fig. 14 for 30×18 and 40×24 meshes.

To construct the reduced models, the number of retained dominant substructural modes is fixed as 30 in every numerical case. Note that, as the number of DOFs increases, the size of reduced models also increases due to the DOF increment in the highest level substructure. The computation times required for calculating the lowest eigenvalues by the original and enhanced AMLS methods are presented in Fig. 15. This result also shows the good computational efficiency of the enhanced AMLS method.

6.2. Reduced models with similar accuracy

For a fair comparison, the computation times of the original and enhanced AMLS methods are measured for the reduced models with similar accuracy. A turbine blade problem in Fig. 16 is considered. Length L is 35 m, thickness is 0.05 m, Young’s modulus E is 210 GPa, Poisson’s ratio ν is 0.3, and density ρ is 7800 kg/m^3 . The detailed geometry is described in Ref. [27]. We use 10300 shell finite elements and 10100 nodes (51308 DOFs). Considering three sub-structural levels (0, 1 and 2), the global structure is partitioned into 19 substructures.

The following numerical cases are considered:

- The original AMLS method is used with the reduced model size of $\bar{N}_p = 1260$ ($N_d = 60$) and $\bar{N}_p = 3100$ ($N_d = 1900$).
- The enhanced AMLS method is used with the reduced model size of $\bar{N}_p = 1260$ ($N_d = 60$).

Fig. 17 shows that the accuracy is similar for the reduced models using the original AMLS method with $\bar{N}_p = 3100$ ($N_d = 1900$) and using the enhanced AMLS method with $\bar{N}_p = 1260$ ($N_d = 60$). Table 9 lists the breakdown of computation time. It is observed that, with similar accuracy, the computation time required for the enhanced AMLS method is less than for the original AMLS method.

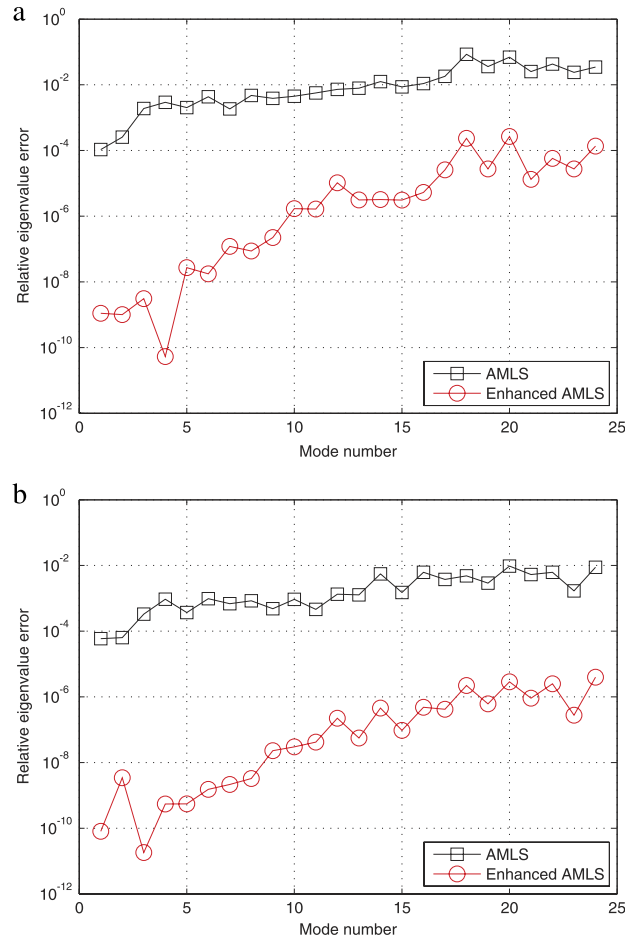


Fig. 13. Relative eigenvalue errors for the hyperboloid shell problem: (a) $N_d = 60$, (b) $N_d = 120$.

Table 9

Computation times for calculating the lowest eigenvalues in the turbine blade problem. The computation times are normalized by the total computation time required for the original AMLS method when $N_d = 60$.

Items	Related equations	Normalized computation times		
		Original AMLS ($N_d = 60$)	Original AMLS ($N_d = 1900$)	Enhanced AMLS ($N_d = 60$)
Transformation procedures	11 and 27			
Solution of the substructural eigenvalue problems	8	0.0736	0.6272	0.0736
Calculation of the multi-level constraint mode matrix $\hat{\Psi}$	13	0.9252	0.9252	0.9252
Solution of the reduced eigenvalue problem	3	0.0012	0.0599	0.0012
Calculation of the residual flexibility matrix \mathbf{F}_{rs} ^a	24	–	–	0.0062
Inverse matrix of the reduced mass matrix \mathbf{M}_p ^a	26	–	–	0.0118
Total		1.0000	1.6123	1.0180

^a Items only required for the enhanced AMLS method.

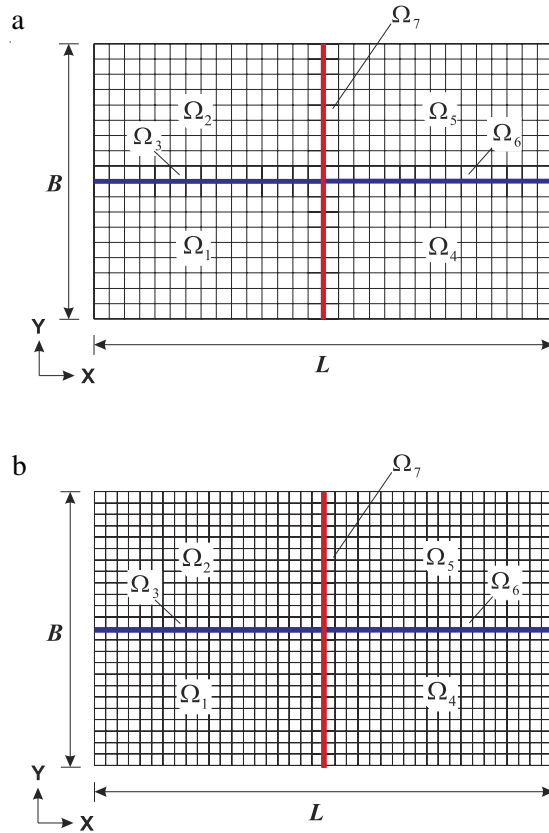


Fig. 14. Two different meshes for the rectangular plate problem with Partition Type A in Fig. 3(a): (a) 30×18 mesh, (b) 40×24 mesh.

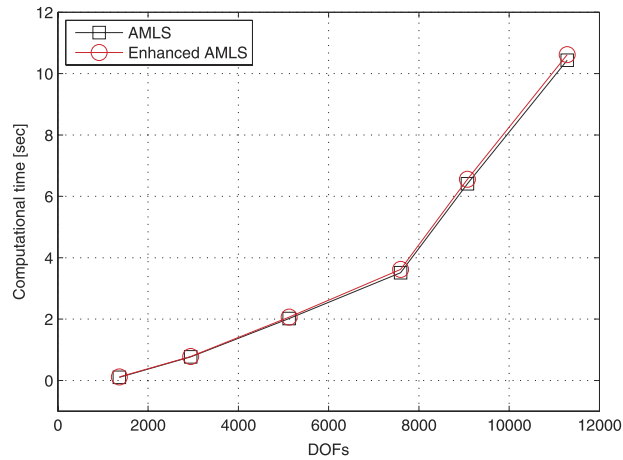


Fig. 15. Computation times depending on the number of DOFs in the rectangular plate problem with Partition Type A in Fig. 3(a).

At this point, it is very important to note that, in this study, we tested the computational cost of the enhanced AMLS method for several FE models with up to 51308 DOFs using our own MATLAB implementation. Therefore, additional tests are required considering various FE models with more than millions of DOFs. Note also that the computational efficiency is crucial to use the enhanced AMLS method as a solver of eigenvalue problems with large DOFs. In order to do that, much more effective computer codes and high performance computers are necessary.

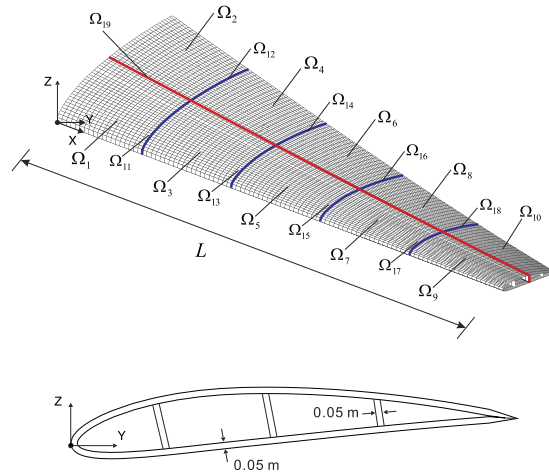


Fig. 16. Turbine blade problem.

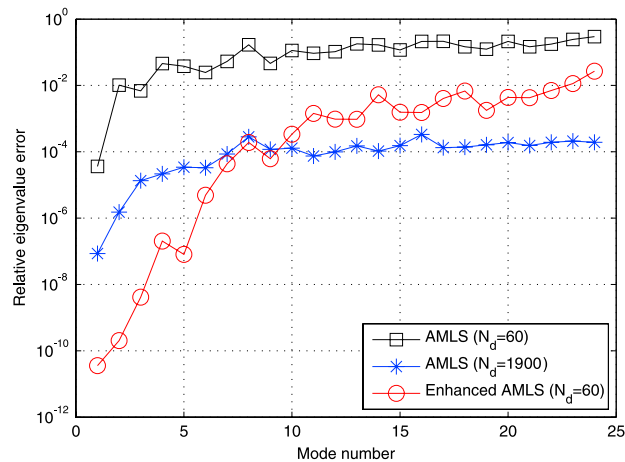


Fig. 17. Relative eigenvalue errors for the turbine blade problem.

7. Conclusions

In this paper, we presented a new component mode synthesis (CMS) method developed by improving the automated multi-level substructuring (AMLS) method. Unlike for the original AMLS method, the residual mode effect is considered in constructing the transformation matrix. As a result, the original AMLS transformation matrix is enhanced by the residual flexibility, in which the unknown eigenvalue is approximated using O'Callahan's approach from the improved reduced system (IRS) method.

The enhanced AMLS method was then developed using this enhanced transformation matrix. As a result, global (original) structural models can be more precisely reduced, and the accuracy of reduced models is dramatically improved. The accuracy improvement of the enhanced AMLS method was demonstrated through numerical examples, and its computational cost was also investigated. However, as mentioned, additional numerical tests on the computational cost of the enhanced AMLS method are necessary considering much larger FE models than those considered in this study.

In order to effectively use the enhanced AMLS method as a solver of eigenvalue problems, it is important to increase its computational efficiency. An optimized algorithm for computer programming would be valuable, and then efficient mode selection and error estimation techniques are essential [28–30]. In addition, the proposed method can be used to reduce the size of system matrices in flexible multi-body systems [31–33].

Acknowledgments

This work was supported by the Basic Science Research Program through the National Research Foundation of Korea (NRF) funded by the Ministry of Education, Science and Technology (No. 2014R1A1A1A05007219), and the Human Resources Development (No. 20134030200300) of the Korea Institute of Energy Technology Evaluation and Planning (KETEP) grant funded by the Korea government Ministry of Trade, Industry and Energy.

References

- [1] R. Guyan, Reduction of stiffness and mass matrices, *AIAA J.* 3 (2) (1965) 380.
- [2] B.M. Irons, Structural eigenvalue problems: elimination of unwanted variables, *AIAA J.* 3 (1965) 961.
- [3] M.I. Friswell, S.D. Garvey, J.E.T. Penny, Model reduction using dynamic and iterated IRS techniques, *J. Sound Vib.* 186 (2) (1995) 311–323.
- [4] Y. Xia, R. Lin, A new iterative order reduction (IOR) method for eigensolutions of large structures, *Internat. J. Numer. Methods Engrg.* 59 (2004) 153–172.
- [5] W. Hurty, Dynamic analysis of structural systems using component modes, *AIAA J.* 3 (4) (1965) 678–685.
- [6] R.R. Craig, M.C.C. Bampton, Coupling of substructures for dynamic analysis, *AIAA J.* 6 (7) (1965) 1313–1319.
- [7] R.H. MacNeal, Hybrid method of component mode synthesis, *Comput. Struct.* 1 (4) (1971) 581–601.
- [8] W.A. Benfield, R.F. Hruda, Vibration analysis of structures by component mode substitution, *AIAA J.* 9 (1971) 1255–1261.
- [9] S. Rubin, Improved component-mode representation for structural dynamic analysis, *AIAA J.* 13 (8) (1975) 995–1006.
- [10] K.C. Park, Y.H. Park, Partitioned component mode synthesis via a flexibility approach, *AIAA J.* 42 (6) (2004) 1236–1245.
- [11] D.J. Rixen, A dual Craig–Bampton method for dynamic substructuring, *J. Comput. Appl. Math.* 168 (1–2) (2004) 383–391.
- [12] K.C. Park, J.G. Kim, P.S. Lee, A mode selection criterion based on flexibility approach in component mode synthesis, in: *Proceeding 53th AIAA/ASME/ASCE/AHS/ASC Structures, Structural Dynamics, and Materials Conference Hawaii, USA, 2012.*
- [13] F. Bourquin, Analysis and comparison of several component mode synthesis methods on one dimensional domains, *Numer. Math.* 58 (1) (1990) 11–33.
- [14] F. Bourquin, Component mode synthesis and eigenvalues of second order operators: discretization and algorithm, *Math. Model. Numer. Anal.* 26 (3) (1992) 385–423.
- [15] F. Bourquin, F. d’Hennezel, Intrinsic component mode synthesis and plate vibrations, *Comput. Struct.* 44 (1–2) (1992) 315–324.
- [16] F. Bourquin, F. d’Hennezel, Numerical study of an intrinsic component mode synthesis method, *Comput. Methods Appl. Mech. Engrg.* 97 (1) (1992) 49–76.
- [17] J.K. Bennighof, R.B. Lehoucq, An automated multi-level substructuring method for eigenspace computation in linear elastodynamics, *SIAM J. Sci. Comput.* 25 (6) (2004) 2084–2106.
- [18] J. O’Callahan, A procedure for an improved reduced system (IRS) model, in: *Proceeding of the 7th International Modal Analysis Conference, CT, Bethel, 1989.*
- [19] M.F. Kaplan, Implementation of automated multi-level substructuring for frequency response analysis of structures (Ph.D. thesis), Department of Aerospace Engineering & Engineering Mechanics, University of Texas at Austin, Austin, TX, 2001.
- [20] J.K. Bennighof, M.F. Kaplan, Frequency sweep analysis using multi-level substructuring, global modes and iteration, in: *Proceedings of the 39th Annual AIAA Structural Dynamics and Materials Conference, Long Beach, CA, 1998.*
- [21] S.H. Boo, J.G. Kim, P.S. Lee, Error estimation for the automated multi-level substructuring method, *Internat. J. Numer. Methods Engrg.* (2015) submitted for publication.
- [22] A. Ibrahimbegovic, H.C. Chen, E.L. Wilson, R.L. Taylor, Ritz method for dynamic analysis of linear systems with non-proportional damping, *Int. J. Earthq. Eng. Struct. Dyn.* 19 (1990) 877–889.
- [23] E.N. Dvorkin, K.J. Bathe, A continuum mechanics based four-node shell element for general nonlinear analysis, *Eng. Comput.* 1 (1) (1984) 77–88.
- [24] K.J. Bathe, E.N. Dvorkin, A formulation of general shell elements—the use of mixed interpolation of tensorial components, *Internat. J. Numer. Methods Engrg.* 22 (3) (1986) 697–722.
- [25] Y. Lee, K.H. Yoon, P.S. Lee, Improving the MITC3 shell finite element by using the Hellinger–Reissner principle, *Comput. Struct.* 110–111 (2012) 93–106.
- [26] Y. Lee, P.S. Lee, K.J. Bathe, The MITC3+ shell finite element and its performance, *Comput. Struct.* 138 (2014) 12–23.
- [27] K.H. Yoon, Y. Lee, P.S. Lee, A continuum mechanics based 3-D beam finite element with warping displacements and its modeling capabilities, *Struct. Eng. Mech.* 43 (4) (2012) 411–437.
- [28] J.G. Kim, K.H. Lee, P.S. Lee, Estimating relative eigenvalue errors in the Craig–Bampton method, *Comput. Struct.* 139 (2014) 54–64.
- [29] J.G. Kim, P.S. Lee, An accurate error estimator for Guyan reduction, *Comput. Methods Appl. Mech. Engrg.* 278 (2014) 1–19.
- [30] A. Ibrahimbegovic, E.L. Wilson, Automated truncation of Ritz vector basis in modal transformation, *ASCE J. Engrg. Mech. Div.* 116 (1990) 2506–2520.
- [31] O.P. Agrawal, A.A. Shabana, Dynamic analysis of multibody systems using component modes, *Comput. Struct.* 21 (6) (1985) 1301–1312.
- [32] J. Gerstmayr, J.A.C. Ambrosio, Component mode synthesis with constant mass and stiffness matrices applied to flexible multibody systems, *Internat. J. Numer. Methods Engrg.* 73 (2008) 1518–1546.
- [33] A. Ibrahimbegovic, R.L. Taylor, H. Lim, Nonlinear dynamics of flexible multibody systems, *Comput. Struct.* 81 (2003) 1113–1132.